Truncated thermal equilibrium distribution for intense beam propagation

Ronald C. Davidson and Hong Qin
Plasma Physics Laboratory, Princeton University, Princeton, New Jersey 08543

Steven M. Lund
Lawrence Livermore National Laboratory, University of California, Livermore, California 94550
(Received 6 December 2002; published 24 February 2003)

An intense charged particle beam with directed kinetic energy $(\gamma_b - 1)m_b c^2$ propagates in the z direction through an applied focusing field with transverse focusing force modeled by $\mathbf{F}_{\rm foc} = -\gamma_b m_b \omega_{\beta\perp}^2 \mathbf{x}_\perp$ in the smooth-focusing approximation. This paper examines properties of the axisymmetric, truncated thermal equilibrium distribution $F_b(r, \mathbf{p}_\perp) = A\exp(-H_\perp/\hat{T}_{\perp b}) \oplus (H_\perp - E_b)$, where A, $\hat{T}_{\perp b}$, and E_b are positive constants, and $H_\perp$ is the Hamiltonian for transverse particle motion. The equilibrium profiles for beam number density, $n_b(r) = \int d^2p F_b(r, \mathbf{p}_\perp)$, and transverse temperature, $T_{\perp b}(r) = [n_b(r)]^{-1} \int d^2p (p_\perp^2/2\gamma_b m_b) F_b(r, \mathbf{p}_\perp)$, are calculated self-consistently including space-charge effects. Several properties of the equilibrium profiles are noteworthy. For example, the beam has a sharp outer edge radius r_b with $n_b(r \geq r_b) = 0$, where r_b depends on the value of $E_b/\hat{T}_{\perp b}$. In addition, unlike the choice of a semi-Gaussian distribution, $F_b^{\rm SG} = A\exp(-p_\perp^2/2\gamma_b m_b \hat{T}_{\perp b}) \oplus (r - r_b)$, the truncated thermal equilibrium distribution $F_b(r, \mathbf{p})$ depends on $(r, \mathbf{p})$ only through the single-particle constant of the motion $H_\perp$ and is therefore a true steady-state solution $(\partial/\partial t = 0)$ of the nonlinear Vlasov-Maxwell equations.

DOI: 10.1103/PhysRevSTAB.6.024402 PACS numbers: 29.27.Bd, 41.85.Ct, 41.85.Ew

I. INTRODUCTION AND THEORETICAL MODEL

This paper makes use of the nonlinear Vlasov-Maxwell equations [1–4] to investigate the properties of self-consistent intense beam equilibria $(\partial/\partial t = 0)$ with a sharp outer beam edge at radius $r = r_b$. The analysis considers an axially continuous charged particle beam made up of particles with charge e_b and rest mass m_b propagating in the z direction with directed axial kinetic energy $(\gamma_b - 1)m_b c^2$, where $\gamma_b = (1 - \beta_b^2)^{-1/2}$ is the relativistic mass factor, $V_b = \beta_b c$ is the average axial velocity of the beam particles, and c is the speed of light *in vacuo*. The applied transverse focusing force on a beam particle is modeled in the smooth-focusing approximation [1–3] by $\mathbf{F}_{\rm foc} = -\gamma_b m_b \omega_{\beta\perp}^2 \mathbf{x}_\perp$, where $\omega_{\beta\perp} = \text{const}$ is the applied focusing frequency, and $\mathbf{x}_\perp = x\hat{\mathbf{e}}_x + y\hat{\mathbf{e}}_y$ is the transverse displacement of a beam particle from the axis. Finally, the particle motion in the beam frame is assumed to be nonrelativistic. The main purpose of the present analysis is to describe a particular choice of self-consistent beam equilibrium distribution function, with a sharp outer beam edge, that can serve as a useful alternative to a semi-Gaussian distribution.

By way of background, particle-in-cell simulations of intense beam propagation [5–9] often make use of an input distribution function, known as a *semi-Gaussian* distribution, in which the phase-space dependence of the transverse distribution function is taken to be of the form

$$F_b^{\rm SG} = \frac{\hat{n}_b}{2\pi\gamma_b m_b \hat{T}_{\perp b}} \exp\left(-\frac{p_\perp^2}{2\gamma_b m_b \hat{T}_{\perp b}}\right) \oplus (r - r_b). \quad (1)$$

Here, $p_\perp = (p_x^2 + p_y^2)^{1/2}$ is the transverse particle momentum, $r = (x^2 + y^2)^{1/2}$ is the radial distance of a particle from the beam axis, $\hat{n}_b$ and $\hat{T}_{\perp b}$ are positive constants, and $\oplus(x)$ is the Heaviside step function defined by $\oplus(x) = +1$ for $x < 0$, and $\oplus(x) = 0$ for $x > 0$. An important feature of Eq. (1) is that the corresponding number density of beam particles, $n_b(r) = \int d^2p_\perp F_b^{\rm SG}$, has the simple uniform-density step-function profile, $n_b(r) = \hat{n}_b \oplus (r - r_b)$, with a sharp beam edge at radius $r = r_b$, and $n_b(r > r_b) = 0$. Another feature of Eq. (1) is that the local transverse temperature within the beam is spatially uniform with $\int d^2p (p_\perp^2/2\gamma_b m_b) F_b^{\rm SG} = \hat{T}_{\perp b} n_b(r)$, where $\hat{T}_{\perp b} = \text{const}$. A disadvantage of Eq. (1), of course, is that an input distribution function such as Eq. (1) does *not* correspond to a quasi-steady-state equilibrium $(\partial/\partial t = 0)$, since $F_b^{\rm SG}$ is not constructed from single-particle constants of the motion [1,2,10]. Because $\partial F_b^{\rm SG}/\partial t \neq 0$, particle-in-cell simulations based on the initial distribution $F_b^{\rm SG}$ can have a significant transient evolution of the distribution function, even in circumstances where the beam propagation is nominally stable [9].

Consistent with the assumptions summarized above, a self-consistent equilibrium solution $(\partial/\partial t = 0)$ to the nonlinear Vlasov-Maxwell equations can be constructed from the single-particle constants of the motion in the equilibrium field configuration. For an axisymmetric beam $(\partial/\partial\theta = 0)$, the constants of the motion involving the transverse particle dynamics correspond to the canonical angular momentum $P_\theta = xp_y - yp_x$, and the transverse Hamiltonian $H_\perp$ defined by

 © 2003 The American Physical Society

$$H_\perp = \frac{p_\perp^2}{2\gamma_b m_b} + \psi(r),$$

where

$$\psi(r) = \frac{1}{2}\gamma_b m_b \omega_{\beta\perp}^2 r^2 + \frac{e_b}{\gamma_b^2}\phi(r) \tag{2}$$

is the effective radial potential. In Eq. (2), the equilibrium space-charge potential $\phi(r)$ is determined self-consistently in terms of the equilibrium distribution function $F_b(r, \mathbf{p}_\perp)$ from Poisson's equation

$$\frac{1}{r}\frac{\partial}{\partial r} r \frac{\partial}{\partial r}\phi(r) = -4\pi e_b \int d^2 p_\perp F_b(r, \mathbf{p}_\perp), \tag{3}$$

where $n_b(r) = \int d^2 p_\perp F_b(r, \mathbf{p}_\perp)$ is the number density of beam particles. In solving Eq. (3), we take $\phi(r = 0) = 0 = \psi(r = 0)$ without loss of generality. Any transverse distribution function $F_b(r, \mathbf{p}_\perp)$ that depends on $(r, \mathbf{p}_\perp)$ only through the variables $H_\perp$ and P_θ is an exact solution to the steady-state nonlinear Vlasov-Maxwell equations [1,2,10]. For a nonrotating beam, this dependence occurs only through the perpendicular Hamiltonian $H_\perp$, i.e.,

$$F_b(r, \mathbf{p}_\perp) = F_b(H_\perp), \tag{4}$$

which is the class of beam equilibria considered in the present analysis.

The organization of this paper is the following. In Sec. II, the truncated thermal equilibrium distribution is examined analytically. The implications of global radial force balance are considered in Sec. III. Finally, in Sec. IV, numerical solutions are obtained for the self-field potential and radial density profile over a wide range of system parameters.

II. TRUNCATED THERMAL EQUILIBRIUM DISTRIBUTION

Equations (2)–(4) have been extensively analyzed in the literature [11–19] for the case of a thermal equilibrium distribution, $F_b(H_\perp) = A' \exp(-H_\perp/\hat{T}_{\perp b})$, and for a waterbag equilibrium distribution, $F_b(H_\perp) = A'' \oplus (H_\perp - E_b)$, where A', A'', $\hat{T}_{\perp b}$, and E_b are positive constants. One characteristic of the thermal equilibrium distribution is that the (bell-shaped) density profile has an exponentially small (but *nonzero*) value beyond the beam edge. While the waterbag equilibrium has a sharp beam edge at radius $r = r_b$, there is no variation of $F_b(H_\perp)$ with energy $H_\perp$ in the beam interior. In the present paper, we combine these two distribution functions into a single so-called *truncated thermal equilibrium* distribution $F_b(H_\perp)$ defined by

$$F_b(H_\perp) = \frac{\hat{n}_b}{(2\pi\gamma_b m_b \hat{T}_{\perp b})[1 - \exp(-E_b/\hat{T}_{\perp b})]} \times \exp(-H_\perp/\hat{T}_{\perp b}) \oplus (H_\perp - E_b). \tag{5}$$

Here, $\hat{n}_b$, $\hat{T}_{\perp b}$, and E_b are positive constants, and $\hat{n}_b \equiv n_b(r = 0)$ can be identified with the on-axis ($r = 0$) value of number density because $\phi(r = 0) = 0 = \psi(r = 0)$ is assumed. Equation (5) is a fully self-consistent equilibrium solution ($\partial/\partial t = 0$) to the nonlinear Vlasov-Maxwell equations within the context of the assumptions enumerated earlier.

Substituting Eq. (5) into the definition of $n_b(r) = 2\pi \int_0^\infty dp_\perp p_\perp F_b(H_\perp)$ and carrying out the integration over $p_\perp$ readily gives the equilibrium density profile

$$n_b(r) = \begin{cases} \hat{n}_b \frac{[\exp(-\psi/\hat{T}_{\perp b}) - \exp(-E_b/\hat{T}_{\perp b})]}{[1 - \exp(-E_b/\hat{T}_{\perp b})]}, & 0 \le r < r_b, \\ 0, & r_b < r \le r_w, \end{cases} \tag{6}$$

where $r_w = \text{const}$ is the radius of a cylindrical, perfectly conducting wall. Here, the outer edge radius of the beam ($r = r_b$) is determined self-consistently in terms of the constant E_b from

$$\psi(r = r_b) = E_b \equiv \psi_b = \text{const}. \tag{7}$$

This follows for the choice of distribution function in Eq. (5) because the particle motion is constrained to $H_\perp < E_b$, or equivalently, $p_\perp^2/2\gamma_b m_b < E_b - \psi(r)$. Therefore, the edge radius r_b is determined from $\psi(r = r_b) = E_b$ (where $p_\perp = 0$), and there are no particles for $r > r_b$. We substitute Eqs. (2) and (6) into Poisson's equation (3). This readily gives the closed nonlinear differential equation for $\psi(r)$,

$$\frac{1}{r}\frac{\partial}{\partial r} r \frac{\partial}{\partial r}\frac{\psi(r)}{\hat{T}_{\perp b}} = \frac{2\gamma_b m_b \omega_{\beta\perp}^2}{\hat{T}_{\perp b}}\left[1 - \hat{s}_b \frac{[\exp(-\psi/\hat{T}_{\perp b}) - \exp(-E_b/\hat{T}_{\perp b})]}{[1 - \exp(-E_b/\hat{T}_{\perp b})]} \oplus (r - r_b)\right]. \tag{8}$$

In Eq. (8), the constant

$$\hat{s}_b = \frac{\hat{\omega}_{pb}^2}{2\gamma_b^2 \omega_{\beta\perp}^2} \tag{9}$$

is a dimensionless measure of the normalized beam intensity, and $\hat{\omega}_{pb} = (4\pi\hat{n}_b e_b^2/\gamma_b m_b)^{1/2}$ is the relativistic plasma frequency at $r = 0$. A careful examination of Eqs. (6) and (8) shows that the condition for existence of a radially confined density profile [the condition for $n_b(r)$ to be a nonincreasing function of r] is that the normalized beam intensity satisfies $\hat{s}_b < 1$. From Eq. (8), the inequality $\hat{s}_b < 1$ assures that $\{r^{-1}(\partial/\partial r)[r\partial\psi/\partial r]\}_{r=0} > 0$ and hence that $n_b(r)$ decreases monotonically as a function of increasing r (see also the discussion on pp. 200–201 of Ref. [1]). Whenever the inequality $\hat{s}_b < 1$ is satisfied, the solution to Eq. (8)

for $\psi(r)$ increases monotonically from $\psi(r=0)=0$ to the value $\psi(r=r_b)=E_b\equiv\psi_b$ at the outer edge of the beam. Correspondingly, from Eq. (6), the number density $n_b(r)$ decreases from the value $n_b(r=0)=\hat{n}_b$ at $r=0$, to $n_b(r=r_b)=0$ at the beam edge.

Other equilibrium properties can also be calculated for the choice of truncated thermal equilibrium distribution in Eq. (5). For example, the transverse pressure profile is defined by $P_{\perp b}(r)=n_b(r)T_{\perp b}(r)=2\pi\int_0^\infty dp_\perp p_\perp(p_\perp^2/2\gamma_b m_b)F_b(H_\perp)$ [10,18]. Making use of Eqs. (5) and (6), and integrating over $p_\perp$, some straightforward algebraic manipulation shows that the transverse temperature profile $T_{\perp b}(r)$ for the choice of distribution function in Eq. (5) is given by

$$T_{\perp b}(r)=\hat{T}_{\perp b}\frac{\{\exp(-\psi/\hat{T}_{\perp b})-[1+(E_b-\psi)/\hat{T}_{\perp b}]\exp(-E_b/\hat{T}_{\perp b})\}}{[\exp(-\psi/\hat{T}_{\perp b})-\exp(-E_b/\hat{T}_{\perp b})]} \tag{10}$$

for $0\le r<r_b$. From $\psi(r=0)=0$, we note from Eq. (10) that the on-axis value of transverse temperature is $T_{\perp b}(r=0)=\hat{T}_{\perp b}\{1-(E_b/\hat{T}_{\perp b})/[\exp(E_b/\hat{T}_{\perp b})-1]\}$. Furthermore, for a finite value of $E_b/\hat{T}_{\perp b}$, it can be shown directly from Eq. (10) that the transverse temperature near the beam edge decreases monotonically to zero value, $T_{\perp b}(r=r_b)=0$, with $T_{\perp b}(r)\simeq(1/2)[E_b-\psi(r)]$ as $r\to r_b$ and $\psi(r)\to E_b=\psi(r_b)$.

For specified values of the dimensionless parameters $\hat{s}_b=\hat{\omega}_{pb}^2/2\gamma_b^2\omega_{\beta\perp}^2$ and $E_b/\hat{T}_{\perp b}$, Eq. (8) can be solved numerically for $\psi(r)/\hat{T}_{\perp b}$, and the corresponding density profile $n_b(r)$ and transverse temperature profile $T_{\perp b}(r)$ determined self-consistently from Eqs. (6) and (10), respectively, over a wide range of system parameters. Of course, in the limiting case $E_b/\hat{T}_{\perp b}\to\infty$, Eqs. (6) and (10) reduce to the bell-shaped density profile, $n_b(r)=\hat{n}_b\exp[-\psi(r)/\hat{T}_{\perp b}]$, and uniform transverse temperature profile, $T_{\perp b}(r)=\hat{T}_{\perp b}=\text{const}$, corresponding to thermal equilibrium [10,18]. On the other hand, as noted earlier, for a finite value of $E_b/\hat{T}_{\perp b}$ the beam equilibrium described by Eqs. (5), (6), (8), and (10) has a sharp radial edge at $r=r_b$ determined from $\psi(r=r_b)=E_b$. Moreover, the density and temperature profiles in Eqs. (6) and (10) decrease monotonically to zero as $r\to r_b$. This is expected for the choice of distribution function in Eq. (5) because the maximum transverse Hamiltonian is $[H_\perp]_{\max}=E_b$, and the radial location $r=r_b$ corresponds to the envelope of turning points in the transverse particle orbits for which $[p_\perp^2]=0$ and $\psi(r=r_b)=E_b$ [see Eq. (2)].

III. GLOBAL RADIAL FORCE BALANCE

Before examining specific numerical solutions to Eqs. (6), (8), and (10), we summarize here an important constraint corresponding to global radial force balance [20,21] satisfied by the entire class of beam equilibria described by Eq. (4). We define the statistical average of a phase function χ by

$$\langle\chi\rangle=\frac{1}{N_b}\int d^2x d^2p\,\chi F_b(H_\perp), \tag{11}$$

where $N_b=\int d^2x d^2p F_b(H_\perp)=2\pi\int_0^{r_b}drrn_b(r)$ is the number of beam particles per unit axial length, and $n_b(r)=2\pi\int_0^\infty dp_\perp p_\perp F_b(H_\perp)$ is the number density. Therefore, from Eq. (11), the mean-square beam radius $R_b^2=\langle r^2\rangle$ and the average transverse kinetic energy $\langle(p_x^2+p_y^2)/2\gamma_b m_b\rangle$ can be expressed as

$$R_b^2=\langle r^2\rangle=\frac{2\pi}{N_b}\int_0^{r_b}drrr^2n_b(r),$$
$$\left\langle\frac{p_x^2+p_y^2}{2\gamma_b m_b}\right\rangle=\langle T_{\perp b}(r)\rangle=\frac{2\pi}{N_b}\int_0^{r_b}drrT_{\perp b}(r)n_b(r), \tag{12}$$

where $n_b(r)T_{\perp b}(r)=P_{\perp b}(r)=2\pi\int_0^\infty dp_\perp p_\perp(p_\perp^2/2\gamma_b m_b)\times b(H_\perp)$ is the transverse pressure profile. For the general class of equilibrium distributions in Eq. (4), it can be shown that local radial force balance on a beam fluid element is given by [10,20,21] $\partial P_{\perp b}/\partial r=-\gamma_b m_b\omega_{\beta\perp}^2 n_b r-(n_b e_b/\gamma_b^2)\partial\phi/\partial r$. Without presenting algebraic details, operating with $(2\pi/N_b)\int_0^{r_b}drr^2\cdots$ gives the exact global radial force balance condition [10,20,21]

$$\gamma_b m_b\omega_{\beta\perp}^2R_b^2=\frac{N_b e_b^2}{\gamma_b^2}+2\langle T_{\perp b}(r)\rangle, \tag{13}$$

where R_b^2 and $\langle T_{\perp b}(r)\rangle$ are defined in Eq. (12).

Equation (13) shows clearly that there are two contributions to the mean-square beam radius $R_b^2=\langle r^2\rangle$. The term proportional to $N_b e_b^2/\gamma_b^2=N_b e_b^2(1-\beta_b^2)$ corresponds to the space-charge contribution $(N_b e_b^2)$ reduced by self-magnetic field effects $(-N_b e_b^2\beta_b^2)$, and the term proportional to $2\langle T_{\perp b}(r)\rangle$ corresponds to the *emittance* contribution, proportional to the average transverse temperature of the beam particles. Indeed, it is instructive to introduce the familiar quantities corresponding to self-field perveance (K_b), smooth-focusing lattice coefficient $(\kappa_{\rm sf})$, and unnormalized beam emittance (ϵ) defined by

$$K_b\equiv\frac{2N_b e_b^2}{\gamma_b^3 m_b\beta_b^2c^2},\qquad \kappa_{\rm sf}\equiv\frac{\omega_{\beta\perp}^2}{\beta_b^2c^2},$$
$$\epsilon^2\equiv4\langle x^2+y^2\rangle\left\langle\frac{p_x^2+p_y^2}{\gamma_b^2m_b^2\beta_b^2c^2}\right\rangle=\frac{8}{\gamma_b m_b\beta_b^2c^2}R_b^2\langle T_{\perp b}(r)\rangle. \tag{14}$$

Then, making use of Eq. (14), the radial force condition in Eq. (13) can be expressed in the equivalent form

$$\left(\kappa_{\rm sf} - \frac{K_b}{2R_b^2}\right)R_b = \frac{\epsilon^2}{4R_b^3}, \tag{15}$$

which is identical to the familiar envelope equation relating the rms beam radius R_b to $\kappa_{\rm sf}$, K_b, and ϵ. For specified values of self-field perveance (K_b), focusing field strength ($\kappa_{\rm sf}$), and transverse emittance (ϵ), Eq. (15) gives a closed expression for the mean-square beam radius,

$$R_b^2 = \frac{K_b}{4\kappa_{\rm sf}} + \left[\left(\frac{K_b}{4\kappa_{\rm sf}}\right)^2 + \frac{\epsilon^2}{4\kappa_{\rm sf}}\right]^{1/2}. \tag{16}$$

The radial force balance condition in Eq. (13), or equivalently, Eq. (15), is applicable to the entire class of self-consistent beam equilibria described by Eq. (4), including the special choice of $F_b(H_\perp)$ in Eq. (5). Moreover, Eqs. (13) and (15) are applicable over the full range of system parameters ranging from *emittance-dominated* beams, where

$$R_b^2 \simeq \frac{2}{\gamma_b m_b \omega_{\beta\perp}^2}\langle T_{\perp b}(r)\rangle = \frac{\epsilon}{2\sqrt{\kappa_{\rm sf}}} \tag{17}$$

for $\langle T_{\perp b}(r)\rangle \gg N_b e_b^2/2\gamma_b^2$ (or $\epsilon \gg K_b/2\sqrt{\kappa_{\rm sf}}$), to *space-charge-dominated* beams, where

$$R_b^2 \simeq \frac{N_b e_b^2}{\gamma_b^3 m_b \omega_{\beta\perp}^2} = \frac{K_b}{2\kappa_{\rm sf}} \tag{18}$$

for $N_b e_b^2/2\gamma_b^2 \gg \langle T_{\perp b}(r)\rangle$ (or $K_b/2\sqrt{\kappa_{\rm sf}} \gg \epsilon$).

In analyzing Eqs. (6), (8), and (10) it is important to recognize the powerful constraint on system parameters imposed by the radial force balance condition in Eq. (13) [or Eq. (15)], which relates R_b^2, N_b, and $\langle T_{\perp b}(r)\rangle$. For example, when solving Eq. (8) for $\psi(r)$ for a specified value of normalized beam intensity $\hat{s}_b = \hat{\omega}_{pb}^2/2\gamma_b^2\omega_{\beta\perp}^2$, the low-intensity regime ($\hat{s}_b \ll 1$) corresponds to an emittance-dominated beam satisfying Eq. (17). On the other hand, the high-intensity limit ($\hat{s}_b \to 1$) corresponds to the space-charge-dominated regime satisfying Eq. (18).

In addition to $\hat{s}_b$, another convenient measure of self-field intensity is provided by the rms-equivalent tune depression ν/ν_0 defined by

$$\frac{\nu}{\nu_0} = \left(1 - \frac{K_b}{2\kappa_{\rm sf}R_b^2}\right)^{1/2} = \left(1 - \frac{N_b e_b^2}{\gamma_b^3 m_b \omega_{\beta\perp}^2 R_b^2}\right)^{1/2}. \tag{19}$$

In the low-intensity regime ($\hat{s}_b \ll 1$ and $K_b/2\kappa_{\rm sf}R_b^2 \ll 1$) note that Eq. (19) reduces to $\nu/\nu_0 \simeq 1 - K_b/4\kappa_{\rm sf}R_b^2$. On the other hand, in the space-charge-dominated limit ($\hat{s}_b \to 1$ and $K_b/2\kappa_{\rm sf}R_b^2 \to 1$), Eq. (19) reduces to $\nu/\nu_0 \to 0$.

IV. EXAMPLES OF EQUILIBRIUM PROFILES

For specified values of the dimensionless parameters $\hat{s}_b = \hat{\omega}_{pb}^2/2\gamma_b^2\omega_{\beta\perp}^2$ and $E_b/\hat{T}_{\perp b}$, Eq. (8) can be solved numerically for the normalized self-field potential $\psi(r)/\hat{T}_{\perp b}$, integrating from $r = 0$ where $\psi(r = 0) = 0 = [\partial\psi/\partial r]_{r=0}$. For specified values of $\hat{s}_b$ and $E_b/\hat{T}_{\perp b}$, note from Poisson's equation (8) that a natural dimensionless radial coordinate is r/r_β where $r_\beta = (2\hat{T}_{\perp b}/\gamma_b m_b \omega_{\beta\perp}^2)^{1/2}$. Once $\psi(r)$ is determined numerically, the edge radius r_b of the beam is obtained from $\psi(r = r_b) = E_b$, and the density profile $n_b(r)$ and transverse temperature profile $T_{\perp b}(r)$ are determined self-consistently from Eqs. (6) and (10), respectively. Analytical solutions to Eq. (8) are accessible in two limiting cases, which are useful to benchmark the numerical solutions. The first case corresponds to a low-intensity (emittance-dominated) beam with $\hat{s}_b \ll 1$ and $\langle T_{\perp b}(r)\rangle \neq 0$. The second case corresponds to a high-intensity (space-charge-dominated) beam with $\hat{s}_b \to 1$ and $\langle T_{\perp b}(r)\rangle \to 0$.

A. Low-intensity beam equilibrium ($\hat{s}_b \ll 1$)

For $\hat{s}_b \ll 1$, the space-charge contribution proportional to $\hat{s}_b$ in Eq. (8) can be neglected to leading order, which gives $\psi(r) \simeq (\gamma_b m_b \omega_{\beta\perp}^2/2)r^2$. We determine r_b from $\psi(r = r_b) = E_b$, which gives $r_b^2 = 2E_b/\gamma_b m_b \omega_{\beta\perp}^2$. Substituting into Eqs. (6) and (10) then gives the density and temperature profiles

$$n_b(r) = \hat{n}_b \frac{\{\exp[-(r^2/r_b^2)(E_b/\hat{T}_{\perp b})] - \exp(-E_b/\hat{T}_{\perp b})\}}{\{1 - \exp(-E_b/\hat{T}_{\perp b})\}} \times \oplus(r - r_b), \tag{20}$$

and

$$T_{\perp b}(r) = \hat{T}_{\perp b} \frac{\{\exp[(-r^2/r_b^2)(E_b/\hat{T}_{\perp b})] - [1 + (E_b/\hat{T}_{\perp b})(1 - r^2/r_b^2)]\exp(-E_b/\hat{T}_{\perp b})\}}{\{\exp[(-r^2/r_b^2)(E_b/\hat{T}_{\perp b})] - \exp(-E_b/\hat{T}_{\perp b})\}} \oplus (r - r_b). \tag{21}$$

Illustrative plots of $n_b(r)/\hat{n}_b$ and $T_{\perp b}(r)/T_{\perp b}(r = 0)$ versus r/r_b are shown in Fig. 1 for the case where $E_b/\hat{T}_{\perp b} = 0.1, 1, 10$. Note from Eqs. (20) and (21) that the beam has a sharp edge at radius $r = r_b$, and that the profiles for $n_b(r)$ and $T_{\perp b}(r)$ approach zero continuously as $r \to r_b$. Furthermore, in the limit $E_b/\hat{T}_{\perp b} \to \infty$, Eqs. (20) and (21) reduce to the Gaussian density profile $n_b(r) = \hat{n}_b \exp(-\gamma_b m_b r^2 \omega_{\beta\perp}^2/2\hat{T}_{\perp b})$ and uniform temperature profile $T_{\perp b}(r) = \hat{T}_{\perp b} = \text{const}$. On the other hand, for $E_b/\hat{T}_{\perp b} \ll 1$, Eqs. (20) and (21) can be approximated by the parabolic profiles $n_b(r) = \hat{n}_b(1 - r^2/r_b^2)$ and $T_{\perp b}(r) = (E_b/2)(1 - r^2/r_b^2)$ for $0 \le r < r_b$.

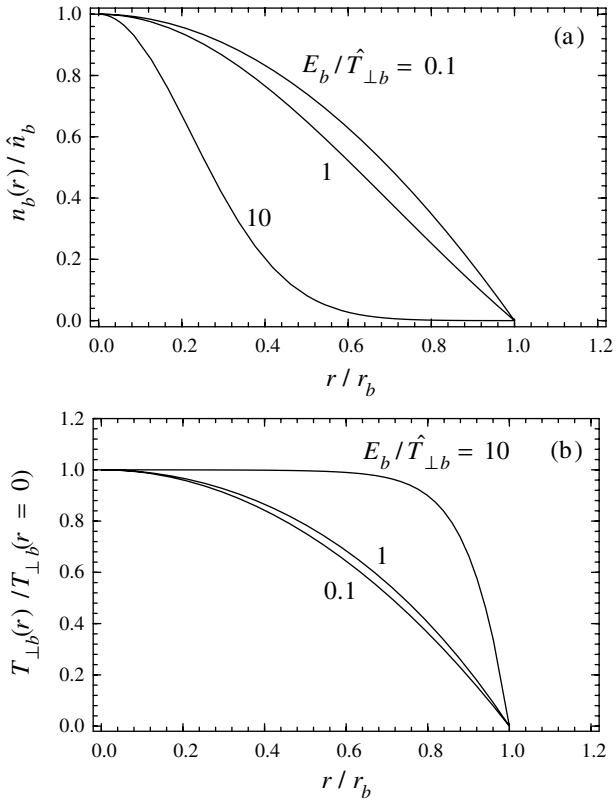

FIG. 1. Plots of normalized (a) density $n_b(r)/\hat{n}_b$ and (b) temperature $T_{\perp b}(r)/T_{\perp b}(r=0)$ versus r/r_b obtained from Eqs. (20) and (21) for $\hat{s}_b \ll 1$, and $E_b/\hat{T}_{\perp b} = 0.1,\ 1,\ 10$.

B. Space-charge-dominated beam equilibrium ($\hat{s}_b \to 1, \langle T_{\perp b}\rangle \to 0$)

As a second limiting case that is analytically tractable, we consider Eqs. (5), (6), (8), and (10) in the cold, space-charge-dominated regime with $\hat{s}_b = \hat{\omega}_{pb}^2/2\gamma_b^2\omega_{\beta\perp}^2 \to 1$, and $\langle T_{\perp b}(r)\rangle \to 0$ corresponding to $\hat{T}_{\perp b} \to 0$ and $E_b \to 0$. In this case, the applied focusing force and the (repulsive) space-charge force exactly cancel in the beam interior, and the solutions to Eqs. (6), (8), and (10) reduce to $\psi(r) = 0$, $T_{\perp b}(r) = 0$, and

$$n_b(r) = \hat{n}_b \oplus (r - r_b) \tag{22}$$

for $0 \le r < r_b$. Note from Eq. (21) and Fig. 2 that the beam density profile is uniform with $n_b(r) = \hat{n}_b = \text{const}$ in the beam interior. Furthermore, for $\hat{s}_b \to 1$, the beam edge radius $r_b = \sqrt{2}R_b$ is readily determined from $r_b^2 = 2N_b e_b^2/\gamma_b^3 m_b \omega_{\beta\perp}^2$ [see Eq. (18)], where $N_b = \hat{n}_b \pi r_b^2$ is the axial line density.

Comparing Figs. 1 and 2, there is a large variation in the shape of the density profile $n_b(r)$ between the low-intensity regime ($\hat{s}_b \ll 1$ in Fig. 1) and the space-charge-dominated regime ($\hat{s}_b \to 1$ in Fig. 2). For general values of $\hat{s}_b$ and $E_b/\hat{T}_{\perp b}$, Eq. (8) can be solved numerically for $\psi(r)$, and the corresponding self-consistent profiles

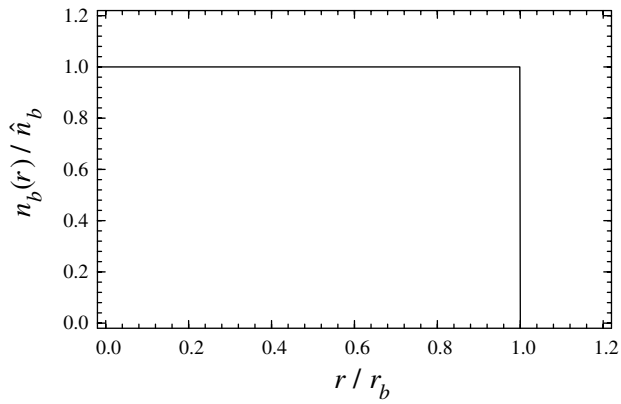

FIG. 2. Plot of normalized density $n_b(r)/\hat{n}_b$ versus r/r_b [Eq. (22)] for space-charge-dominated beam with $\hat{s}_b \to 1$.

for $n_b(r)$ and $T_{\perp b}(r)$ determined from Eqs. (6) and (10). Typical numerical solutions are illustrated in Figs. 3–6.

Shown in Fig. 3 are plots of the normalized potential $\psi(r)/\hat{T}_{\perp b}$ versus r/r_b obtained numerically from Eq. (8) for several values of normalized beam intensity $\hat{s}_b = \hat{\omega}_{pb}^2/2\gamma_b^2\omega_{\beta\perp}^2$ and values of $E_b/\hat{T}_{\perp b}$ ranging from 0.1 to 10. The corresponding values of tune depression ν/ν_0 [Eq. (19)] are also shown in Fig. 3. Note from Fig. 3 that $\psi(r)$ increases monotonically from $\psi(r=0) = 0$ to $\psi(r = r_b) = E_b$ at the beam edge. Moreover, comparing Figs. 3(a) and 3(b), $\psi(r)$ is nearly parabolic in the beam interior when $\hat{s}_b \ll 1$ [$\hat{s}_b = 0.1$ in Fig. 3(a)], whereas $\psi(r)$ remains close to zero in the beam interior, and increases rapidly to $\psi(r_b) = E_b$ near the beam edge when $\hat{s}_b \to 1$ [$\hat{s}_b = 0.999$ in Fig. 3(d)]. At high space-charge intensity with $\hat{s}_b \to 1$, note from Fig. 3(d) that the effective potential $\psi(r) = \gamma_b m_b \omega_{\beta\perp}^2 r^2/2 + (e_b/\gamma_b^2)\phi(r)$ is approximately zero over a broad interior region of the beam, corresponding to a near cancellation of the applied focusing force and the (repulsive) self-field force. The solutions for $\psi(r)/\hat{T}_{\perp b}$ in Fig. 3 are used to determine the corresponding self-consistent density and temperature profiles from Eqs. (6) and (10). The results are illustrated in Figs. 4 and 5 where the normalized density $n_b(r)\pi r_b^2/N_b$ and temperature $T_{\perp b}(r)/\hat{T}_{\perp b}$ are plotted versus r/r_b for values of $\hat{s}_b$ and $E_b/\hat{T}_{\perp b}$ similar to those in Fig. 3. Note from Fig. 4(a) that $n_b(r)$ has a diffuse, bell-shaped profile for $\hat{s}_b = 0.1$, whereas in Fig. 4(d) $n_b(r)$ has an extended flattop profile in the beam interior for $\hat{s}_b = 0.999$, as expected. Moreover, from Fig. 5, the transverse temperature profile $T_{\perp b}(r)$ decreases rather abruptly to zero at the beam edge ($r = r_b$), although $T_{\perp b}(r)$ tends to be relatively uniform in the beam interior for $E_b/\hat{T}_{\perp b} > 2$.

Finally, we have made use of Eqs. (6)–(8) and (12) to determine the edge radius r_b and rms beam radius R_b over a range of system parameters $\hat{s}_b$ and $E_b/\hat{T}_{\perp b}$. Shown in Fig. 6 are plots of (a) r_b/R_b versus $\hat{s}_b$ and (b) r_b/R_b versus ν/ν_0 obtained from Eqs. (6)–(8) and Eqs. (12) and (19)

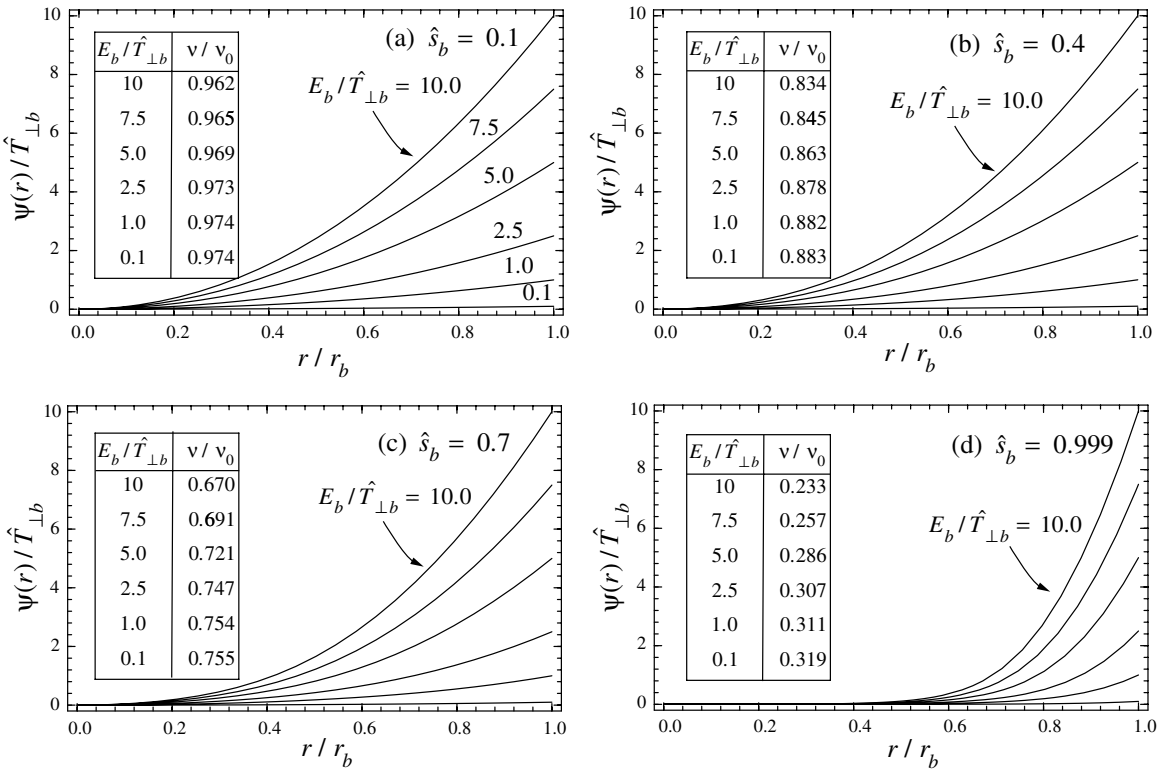

FIG. 3. Plots of normalized potential $\psi(r)/\hat{T}_{\perp b}$ versus r/r_b obtained from Eq. (8) for (a) $\hat{s}_b = 0.1$, (b) $\hat{s}_b = 0.4$, (c) $\hat{s}_b = 0.7$, and (d) $\hat{s}_b = 0.999$, and values of $E_b/\hat{T}_{\perp b}$ corresponding to $E_b/\hat{T}_{\perp b} = 10$, 7.5, 5.0, 2.5, 1.0, 0.1. The corresponding values of tune depression ν/ν_0 [Eq. (19)] are also shown in the figure.

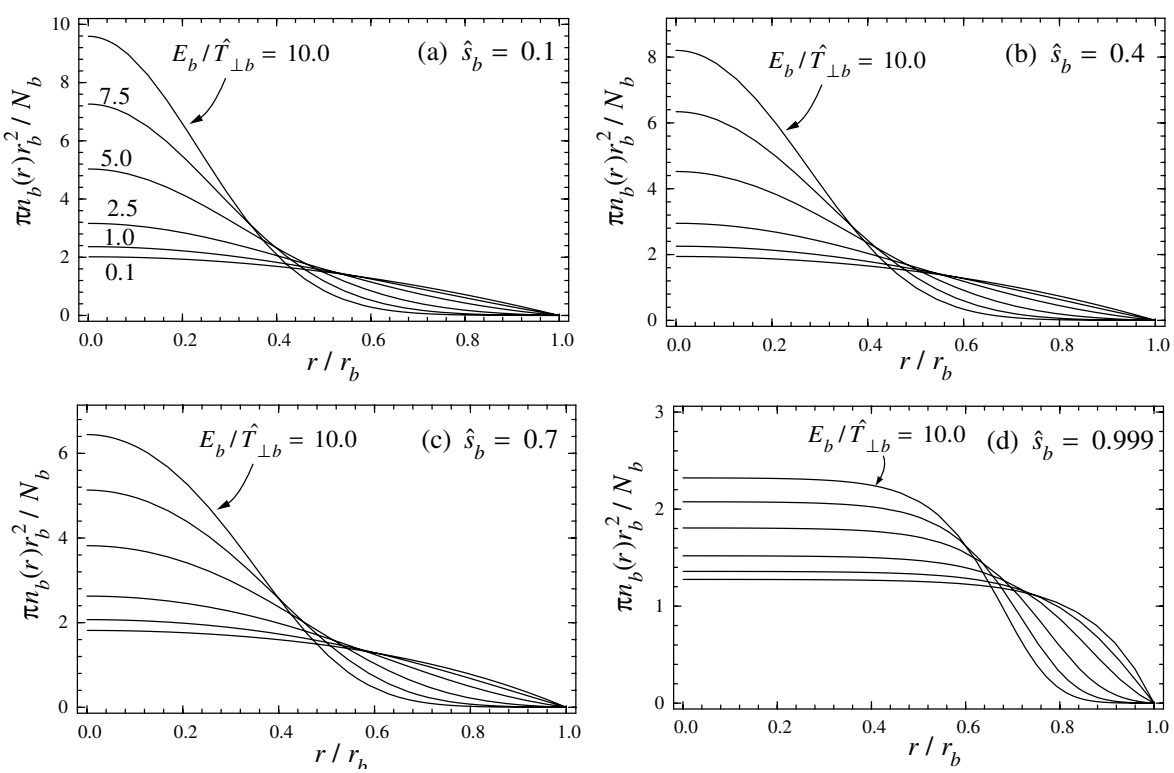

FIG. 4. Plots of normalized density profile $n_b(r)\pi r_b^2/N_b$ versus r/r_b obtained from Eqs. (6) and (8) for (a) $\hat{s}_b = 0.1$, (b) $\hat{s}_b = 0.4$, (c) $\hat{s}_b = 0.7$, and (d) $\hat{s}_b = 0.999$, and several values of $E_b/\hat{T}_{\perp b}$ and ν/ν_0 identical to those in Fig. 3.

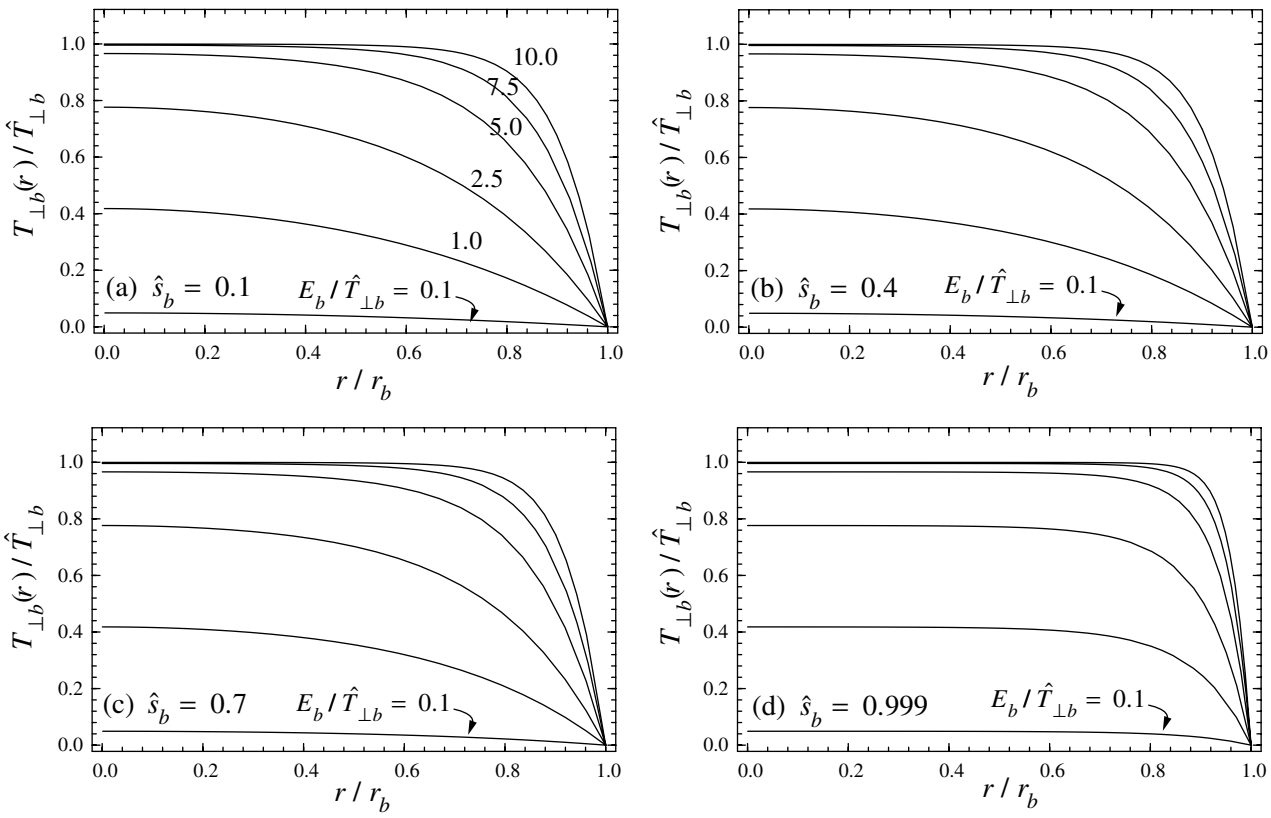

FIG. 5. Plots of normalized temperature profile $T_{\perp b}(r)/\hat{T}_{\perp b}$ versus r/r_b obtained from Eqs. (8) and (10) for (a) $\hat{s}_b = 0.1$, (b) $\hat{s}_b = 0.4$, (c) $\hat{s}_b = 0.7$, and (d) $\hat{s}_b = 0.999$, and several values of $E_b/\hat{T}_{\perp b}$ and ν/ν_0 identical to those in Fig. 3.

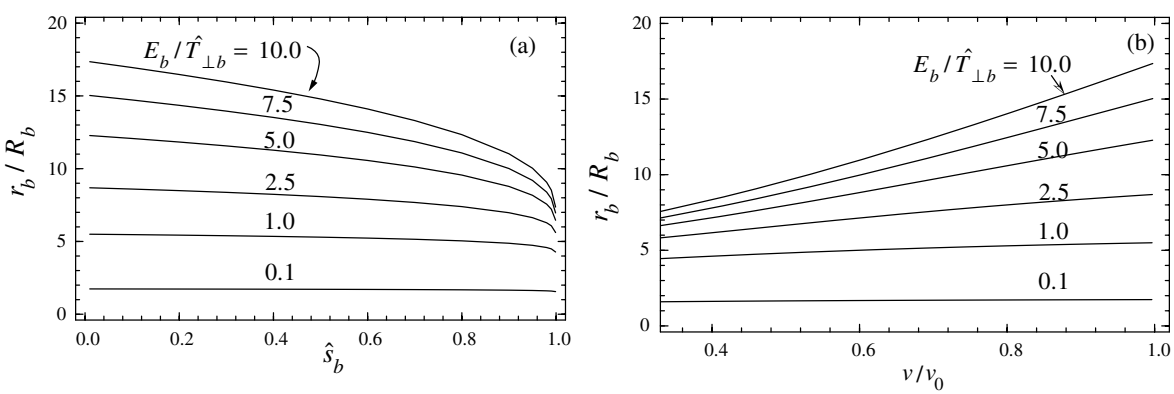

FIG. 6. Plots of normalized edge radius (a) r_b/R_b versus $\hat{s}_b$ and (b) r_b/R_b versus ν/ν_0 obtained from Eqs. (6)–(8) and Eqs. (12) and (19) for several values of $E_b/\hat{T}_{\perp b}$ ranging from 0.1 to 10.

for several values of $E_b/\hat{T}_{\perp b}$. Note from Fig. 6 that r_b/R_b is a slowly varying function of $\hat{s}_b$ and ν/ν_0 and increases as $E_b/\hat{T}_{\perp b}$ is increased.

V. CONCLUSIONS

In this paper, we examined properties of the axisymmetric truncated thermal equilibrium distribution defined in Eq. (5). General equilibrium properties were discussed in Secs. II and III, and expressions for the density profile $n_b(r)$ and transverse temperature profile $T_{\perp b}(r)$ were derived in terms of the effective potential $\psi(r)$ [see Eqs. (6) and (10)], where $\psi(r)$ solves the nonlinear Poisson equation (8). Detailed numerical solutions to Eqs. (6), (8), and (10) were presented in Sec. IV for a wide range of dimensionless system parameters corresponding to $s_b = \hat{\omega}_{pb}^2/2\gamma_b^2\omega_{\beta\perp}^2$ and $E_b/\hat{T}_{\perp b}$. Several properties of the equilibrium profiles are noteworthy. For example, the beam has a sharp outer edge radius r_b with $n_b(r \geq r_b) = 0$, where r_b depends on the value of

$E_b/\hat{T}_{\perp b}$. In addition, unlike the choice of a semi-Gaussian distribution, $F_b^{\rm SG} = A\exp(-p_\perp^2/2\gamma_b m_b \hat{T}_{\perp b}) \times \oplus(r - r_b)$, the truncated thermal equilibrium distribution in Eq. (5) depends on $(r, \mathbf{p}_\perp)$ only through the single particle constant of the motion $H_\perp$ and is therefore a true steady-state solution $(\partial/\partial t = 0)$ of the nonlinear Vlasov-Maxwell equations. It is anticipated that the choice of distribution function in Eq. (5) will be useful in implementing particle-in-cell simulations of intense beams without large initial transient evolutions and incorporating the important feature of a beam with a sharp outer edge radius.

Finally, it should be pointed out that the present analysis also applies to an intense rotating beam propagating through a uniform solenoidal magnetic field $B_0\hat{\mathbf{e}}_z$ in circumstances where the beam particles have zero average canonical angular momentum $\langle P_\theta\rangle = r(\langle p_\theta\rangle + e_b B_0 r/2c) = 0$. In this case, we make the replacement $\omega_{\beta\perp} \rightarrow \omega_{cb}/2$, and all variables are interpreted as being measured in a frame of reference rotating with the Larmor frequency $\omega_{cb}/2 = -e_b B_0/2\gamma_b m_b c$ relative to the laboratory frame.

ACKNOWLEDGMENTS

This research was supported by the Department of Energy.

[1] R.C. Davidson and H. Qin, *Physics of Intense Charged Particle Beams in High Energy Accelerators* (World Scientific, Singapore, 2001), and references therein.

[2] R.C. Davidson, *Physics of Nonneutral Plasmas* (World Scientific, Singapore, 2001), and references therein.

[3] A.W. Chao, *Physics of Collective Beam Instabilities in High Energy Accelerators* (Wiley, New York, 1993).

[4] M. Reiser, *Theory and Design of Collective Particle Beams* (Wiley, New York, 1994).

[5] A. Friedman, D. P. Grote, and I. Haber, Phys. Fluids B **4**, 2203 (1992).

[6] S. M. Lund, J. J. Barnard, G. D. Craig, A. Friedman, D. P. Grote, T. S. Sangster, W. M. Sharp, S. Eylon, T. T. Fessenden, E. Henestroza, S. Yu, and I. Jaber, Nucl. Instrum. Methods Phys. Res., Sect. A **415**, 345 (1998).

[7] A. Friedman, J. J. Barnard, D. P. Grote, and I. Haber, Nucl. Instrum. Methods Phys. Res., Sect. A **415**, 455 (1998).

[8] I. Haber, A. Friedman, D. P. Grote, S. M. Lund, and R. A. Kishek, Phys. Plasmas **6**, 2254 (1999).

[9] E. Sonnendrucker, J. J. Barnard, A. Friedman, D. P. Grote, and S. M. Lund, Nucl. Instrum. Methods Phys. Res., Sect. A **464**, 470 (2001); R. A. Kishek, P. G. O'Shea, and M. Reiser, Phys. Rev. Lett. **85**, 4514 (2000).

[10] See, for example, Chaps. 5 and 7 of Ref. [1].

[11] R.C. Davidson and N. A. Krall, Phys. Fluids **13**, 1543 (1970).

[12] I. Hofmann and J. Struckmeier, Part. Accel. **21**, 69 (1987).

[13] J. Struckmeier and I. Hofmann, Part. Accel. **39**, 219 (1992).

[14] R.C. Davidson and S. M. Lund, in *Advances in Plasma Physics*, edited by N. J. Fisch, AIP Conf. Proc. No. 314 (AIP, New York, 1994), p. 1.

[15] N. Brown and M. Reiser, Phys. Plasmas **2**, 965 (1995).

[16] R.C. Davidson and C. Chen, Part. Accel. **59**, 175 (1998).

[17] R.C. Davidson, Phys. Rev. Lett. **81**, 991 (1998).

[18] R.C. Davidson and H. Qin, Phys. Rev. ST Accel. Beams **2**, 114401 (1999).

[19] D. H. E. Dubin and T. M. O'Neil, Rev. Mod. Phys. **71**, 87 (1999).

[20] R.C. Davidson, W.W. Lee, and P. H. Stoltz, Phys. Plasmas **5**, 279 (1998).

[21] See, for example, Chap. 6 of Ref. [1].